Manuscript prepared for The Cryosphere
with version 5.0 of the LaTeX class copernicus.cls.
Date: 4 June 2014

Impact of anomalies in the surrounding oceanic conditions on 2007-2012 Greenland Ice Sheet surface mass balance using the regional climate model MAR

B. Noël[1,2], X. Fettweis[1], W.J. van de Berg[2], M.R. van den Broeke[2], and M. Erpicum[1]

[1]Department of Geography, University of Liège, Belgium
[2]Institute for Marine and Atmospheric research Utrecht, University of Utrecht, Netherlands

Correspondence to: Brice Noël (B.P.Y.Noel@uu.nl)

Abstract.

During recent summers (2007-2012), several surface melt records were broken over the Greenland Ice Sheet (GrIS). The extreme summer melt resulted in part from a persistent negative phase of the North-Atlantic Oscillation (NAO), favouring warmer conditions than normal over the GrIS. In addition, it has been proposed that large anomalies in sea ice cover (SIC) and sea surface temperature (SST) may partially explain recent anomalous GrIS surface melt. To assess the direct impact of 2007-2012 SIC and SST anomalies on GrIS surface mass balance (SMB), a set of sensitivity experiments was carried out with the regional climate model MAR. These simulations reveal that perturbations in SST and SIC in the seas surrounding Greenland do not considerably impact GrIS SMB as a result of the katabatic winds blocking effect. These offshore directed winds prevent oceanic near-surface air, influenced by SIC and SST anomalies, from penetrating far inland. Therefore, the ice sheet SMB response is restricted to coastal regions, where katabatic winds cease. However, anomalies in SIC and SST might have indirectly affected the surface melt by changing the general circulation in the North Atlantic region, hence favouring more frequent warm air advection towards the GrIS.

1 Introduction

The Greenland Ice Sheet (GrIS) is the world's second largest ice sheet with an area of $\approx$ 1.7 million km², covering more than 80% of Greenland. The GrIS contains almost 10% of the Earth's total fresh water, accounting for a $\approx$ 7 m global mean sea level rise if completely melted. The ice sheet thickness is about 3 km at its centre and progressively decreases towards the ice-free tundra regions (Hanna et al., 2009). Previous work has shown that the GrIS is strongly sensitive to climate warming in response to a combination of natural and anthropogenic forcing. The GrIS mass loss has accelerated over the last decades (Rignot et al., 2011; Enderlin and Howat, 2013; Fettweis et al., 2013b; Wouters et al., 2013) as a result of enhanced GrIS surface melting and iceberg calving (Hanna et al., 2009; Van den Broeke et al., 2009). These ablation processes contribute to $\approx$ 25% of ongoing global sea level rise (Shepherd et al., 2012), affecting coastal regions worldwide. Moreover, by increasing the discharge of fresh meltwater into the Atlantic Ocean and lowering its salinity, GrIS mass loss has the potential to weaken the Atlantic thermohaline circulation (Hanna et al., 2009), partly mitigating projected climate warming in north-western Europe.

Since 2007, several melt records were broken over the GrIS (Hanna et al., 2013a). In particular, July 2012 was characterized by the largest melt extent ever recorded during the satellite era, affecting 97% of the ice sheet surface (Tedesco et al., 2013). To explain these events, several hypotheses have been put forward in recent studies. Anomalous atmospheric forcing, attributed to the persistent 2007-2012 negative phase of the North Atlantic Oscillation (NAO) in summer, has favoured warmer and drier conditions over the ice sheet, enhancing surface melting (Fettweis et al., 2013b). The NAO phase is determined on the basis of the North Atlantic Oscillation Index (NAOI), computed as the normalized pressure difference between Gibraltar and Reykjavik (Jones et al., 1997; Osborn, 2004; Fettweis, 2007). A negative NAO is characterized by less intense westerly flow in mid-latitudes, resulting from weakening of both the Icelandic Low and the Azores High. This leads to strengthening of the south-westerly flow of subtropical air towards the GrIS (Fettweis, 2007). According to Fettweis et al. (2013b), about 70% of

the recent surface melt increase can be attributed to the NAO-induced southwesterly warm air advection towards the western GrIS (Box et al., 2012). The remaining 30% might be explained by long-term anthropogenic warming in the Arctic (Fettweis et al., 2013b).

Oceanic forcing, i.e. changes in sea ice cover (SIC) and sea surface temperature (SST) surrounding Greenland, could have contributed to GrIS SMB decline. In this study, a distinction between the "direct" and the "indirect" impact of oceanic forcing on GrIS SMB is discribed. Direct oceanic forcing is defined as the local (i.e. around Greenland) impact of SIC and/or SST anomalies on near-surface air temperature and moisture, without considering feedbacks on the general circulation. Conversely, the indirect forcing takes into account the SIC and/or SST-induced general circulation variations (Overland et al., 2012) and their potential influence on the atmospheric conditions above Greenland.

In previous studies, the direct influence of oceanic forcing on GrIS SMB was estimated from model sensitivity experiments with the regional climate model MAR (Modèle Atmosphérique Régional) forced by ERA-Interim reanalyses. These experiments were based on imposing individual SST variations (Hanna et al., 2009) or combining SIC-SST perturbations (Hanna et al., 2013a). The first experiment suggested that individual SST variations ($\pm$2ºC) can not fully explain the GrIS melt record observed in the summer of 2007 (Hanna et al., 2009). In the second experiment, Hanna et al. (2013a) used the climatological mean SST and SIC during 1979-1994 instead of 2012 observations to prescribe oceanic conditions in MAR. They stressed that a combination of SIC and SST anomalies did not significantly influence GrIS SMB in the summer of 2012. In addition, Hanna et al. (2013b) stated that perturbations in oceanic conditions might be partly responsible for the recent shift to abnormal negative NAO phase. This shift might contribute to large-scale circulation changes, potentially affecting GrIS SMB (Overland and Wang, 2010; Jaiser et al., 2012). To evaluate both the direct and indirect impact of oceanic forcing on GrIS SMB, Day et al. (2013) conducted 2 sensitivity experiments, consisting of an individual SIC retreat and a combination of SIC reduction and rise in SST, over a 30 year period. In their study, they used the regional climate model HadRM3, forced every 6 hours by the global circulation model HadAM3. Regarding the oceanic conditions, monthly mean SIC and SST, averaged over 2061-2090 and based on the A1B scenario, were used to force HadRM3 and HadAM3. The surface climate variables, supplied by HadRM3 for both experiments, were then used to compute runoff over the GrIS with the ice dynamics ITM SMB model. The comparison with a reference run, characterized by present-day SST and monthly mean SIC covering 1961-1990, allowed Day et al. (2013) to isolate the effect of SIC and combined SIC-SST anomalies on GrIS SMB. The results indicate that an individual SIC reduction leads to a winter precipitation increase, spatially restricted to the centre and the eastern parts of the GrIS. This enhanced accumulation results from stronger evaporation over the ice-free ocean. During summer, a SIC withdrawal weakens North Atlantic cyclonic activity, lowering precipitation over the southern GrIS (Hoskins and Hodges, 2002; Day et al., 2013). The higher winter precipitation increases surface albedo, reducing summer runoff and hence resulting in a positive SMB anomaly. In contrast, a combined SIC-SST forcing leads to a warmer and wetter atmosphere, increasing both winter precipitation and summer surface melting over the GrIS. However, the mass gain is exceeded by enhanced runoff, resulting in a net decrease in SMB (Day et al., 2013).

In spite of these previous studies, large uncertainties remain in the direct oceanic forcing's impact on GrIS SMB. In their experiments, Hanna et al. (2009, 2013a) used a small integration domain ($\approx$ 6.3 x 10^6 km^2), including only a narrow band of oceanic pixels around the GrIS. Consequently, oceanic pixels located close to the edges of the regional model domain are strongly affected by the lateral boundary forcing, potentially suppressing the oceanic impact on the atmospheric conditions. The integration domain area selected for this study (Fig. 1) is twice as large ($\approx$ 13.2 x 10^6 km^2) and extends 300 km further from the ice sheet in the northward and southward directions, 550 km eastwards as well as 950 km towards the west. In addition, both previous studies only analysed a single year, prescribing oceanic anomalies from May to September. Despite Day et al. (2013) considered both the direct and indirect impact of oceanic forcing on GrIS SMB, HadRM3 significantly underestimates total precipitation and ITM SMB overestimates runoff. This might biase the resulting modelled SMB sensitivity to oceanic perturbations. Finally, monthly mean SIC and SST were prescribed in HadRM3, which do not resolve interdiurnal dynamics of oceanic forcing, allowing no consideration of the actual oceanic events and their influence on the atmospheric conditions. As a result, these previously published sensitivity experiments might not provide sufficiently large oceanic forcing to generate a significant impact on GrIS SMB.

This study aims to evaluate whether isolated or coupled SIC and SST anomalies could account for major GrIS SMB perturbations by prescribing modified oceanic conditions within the MAR domain. The simulations are carried out using MAR forcing at 40 km spatial resolution, covering a wider domain than in Hanna et al. (2009, 2013a). Furthermore, MAR presents minor contemporary biases since it has been especially developed to model GrIS SMB (Fettweis, 2007). Our sensitivity experiments are not restricted to the melting season and 6-hourly anomalies in SIC and SST are prescribed in MAR for 2007-2012, instead of fixed monthly mean values.

In Section 2, MAR is briefly introduced as well as the reference and sensitivity simulations. Section 3 describes the impacts of SIC and/or SST anomalies on GrIS SMB. The impact of oceanic forcing on the katabatic wind intensity is discussed in Section 4, followed by conclusions in Section 5.

2 Model and set-up

2.1 The regional climate model MAR

MAR consists of a 3-D atmospheric model that estimates the evolution of the coupled land-atmosphere system resulting from radiative and atmospheric forcing within the integration domain boundaries (Gallée and Schayes, 1994). MAR is coupled to the 1-D module SISVAT (Soil Ice Snow Vegetation Atmosphere Transfer) (Gallée and Schayes, 1994; Ridder and Gallée, 1998), which simulates mass and energy fluxes between the surface-vegetation-atmosphere system. SISVAT includes a 1-D multi-layered snow model, based on the CEN (Centre d'Etudes de la Neige) snow model CROCUS (Brun et al., 1992), which computes the energy fluxes between the sea ice, the ice sheet surface, the snow-covered tundra and the atmosphere (Gallée et al., 2001; Fettweis, 2007). CROCUS consists of a thermodynamic and water balance module including sub-modules for meltwater refreezing, snow metamorphism, snow/ice discretization and surface albedo (Brun et al., 1992; Gallée et al., 2001). Drifting snow is not considered as its variability is assumed to have a minor effect on SMB relative to other components (Lenaerts et al., 2012).

MAR's ability to model GrIS SMB was demonstrated by comparing MAR outputs (Fettweis, 2007) with in-situ measurements (Lefebre et al., 2003, 2005; Gallée et al., 2005) and satellite observations (Fettweis et al., 2005, 2011; Tedesco and Fettweis, 2012). By simulating GrIS SMB using different spatial resolutions, ranging from 15 to 50 km over 1990-2010, Franco et al. (2012) stressed that spatial resolution has no significant impact on the modelled integrated GrIS SMB.

2.2 Set-up of MAR simulations

ERA-Interim reanalysis data (Stark et al., 2007; Dee et al., 2011) are used to force MAR at its lateral boundaries every 6 hours over 2007-2012. The reanalysis is available at a 0.75° x 0.75° spatial resolution.

Since MAR is not coupled to an oceanic model, the oceanic surface conditions, i.e. SIC and SST, are also prescribed in MAR by ERA-Interim. The ice sheet topography, based on Bamber et al. (2013), is kept fixed. The integration domain, depicted in Fig. 1, extends 900 km around the GrIS margins a) to include the neighbouring sea ice and oceans; b) to avoid direct influence of lateral forcing on simulated GrIS SMB. This research is based on MAR version 2 (MARv2), including the set-ups used in Fettweis et al. (2013b).

2.3 Reference run and sensitivity experiments

The reference simulation covers the period 2002-2012. The five first years were used to spin-up the snow model since a proper snow cover initialization, driving the surface albedo conditions and the bare ice areas location, is essential to accurately model GrIS SMB (Lefebre et al., 2005). The sensitivity experiments are branched from the reference run in 2007. Therefore, only the 2007-2012 period is considered in this study. ERA-Interim SIC and SST 6-hourly fields are prescribed in MAR for the reference simulation (Fig. 1 (a,d)). The atmospheric boundary conditions are likewise imposed by ERA-Interim and remains identical in each sensitivity experiment. This underlines the fact that the conducted sensitivity experiments only account for the direct and local (i.e. around Greenland) oceanic impact on GrIS SMB, since no oceanic forcing feedbacks on the general circulation is considered.

2.3.1 SIC anomaly forcing

In the SIC sensitivity experiments, SIC of each oceanic grid cell is replaced by the maximum (resp. minimum) SIC value from a distance range of 3 to 6 grid cells surrounding the current one. This adjustment is applied on the 6-hourly SIC field from ERA-Interim. As a result, SIC is progressively increased (resp. decreased) in 3 or 6 peripheral grid cells, i.e. by 120 or 240 km of horizontal distance, extending outward/inward from the sea ice boundary. This method avoids abrupt and hence unrealistic changes in SIC values between adjacent ice-free and ice-covered oceanic grid cells (Fig. 1 (b,c)). These experiments are referred to as SIC ± 3 and SIC ± 6 in the following sections.

To prevent sea ice from obtaining a surface temperature (ST) higher than the melting point (0ºC) and open-water characterized by a ST lower than the assumed salt water freezing point (-3ºC), a ST correction is applied to each pixel subjected to SIC change, computed as:

$$ST'_{(i,j)} = SIC_{(i,j)} \cdot \min(ST_{melting}, ST_{(i,j)}) + (1\text{-}SIC_{(i,j)}) \cdot \max(ST_{freezing}, ST_{(i,j)})$$

where $ST'_{(i,j)}$ is the corrected surface temperature in ºC for the pixel (i,j) ; $SIC_{(i,j)}$ is the new computed SIC of the pixel (i,j) ; $ST_{(i,j)}$ is the pixel (i,j) uncorrected surface temperature in ºC ; $ST_{melting}$ is the melting point (0ºC) while $ST_{freezing}$ is the salt water freezing point (-3ºC).

2.3.2 SST anomaly forcing

In the SST experiments, 6-hourly SST prescribed by ERA-Interim over 2007-2012, is increased (resp. decreased) by 2 or 4ºC over the ice-free ocean (Fig. 1 (e,f)). These experiments are called SST ± 2 and SST ± 4 subsequently. For a SST reduction, ice-free oceanic grid cells are converted into ice covered grid cells when ST drops below the assumed salt water freezing point (-3ºC). For sea ice covered grid cells, the ST is limited to the melting point (0 ºC) to prevent any SIC change.

2.3.3 Combined SIC-SST anomaly forcing

For the combined forcing experiments, an increase (resp. decrease) in SIC is combined with a decrease (resp. increase) in SST to consider the sea ice insulation feedback. Both 6-hourly SIC and SST anomalies are computed according to Subsections 2.3.1 and 2.3.2, respectively. These experiments are named SIC ± 3 / SST ∓ 2 and SIC ± 6 / SST ∓ 4 in the following sections.

2.3.4 Magnitude of perturbations in oceanic conditions

To assess the magnitude of the perturbations in the oceanic conditions applied in our sensitivity experiments, Tab. 1 lists both the observed and modelled June-July-August (JJA) SST and SIC. The annual mean integrated SIC is computed for the whole model domain whereas the annual mean SST is calculated for the region confined by the black box in Fig. 1. This area was selected because it remains free of sea ice in all experiments, hence excluding numerical artefacts introduced by differences in open ocean area. The 1979-2000 period is used as a reference, because summer SIC has declined and SST has risen since 2001.

The sensitivity experiments represent a 2.5 to 5 times higher (resp. lower) anomaly in SIC (+3, +6; resp. -3, -6) and/or SST (-2, -4; resp. +2, +4) compared to the JJA mean anomaly between both the reference oceanic conditions for 2007-2012 and the observations covering 1979-2000. This underlines the larger perturbation in oceanic forcing applied in our study relative to previous work.

3 Results

This study focuses on the direct impact of local SIC-SST anomalies on the annual mean cumulated GrIS SMB. No oceanic forcing feedback on the general circulation is considered since lateral atmospheric forcing is kept unchanged for each experiment. Hereafter, only anomalies in precipitation and runoff are discussed, since these components are the main drivers of GrIS SMB variability (Box et al., 2004). The anomalies in the annual mean SMB components are listed in Tab. 2, showing significant anomalies in bold. The significance was evaluated using a one-sided Student's t-test with a 95% degree of confidence, based on the differences in SMB components between sensitivity experiments and the reference simulation for 2007-2012.

3.1 SIC sensitivity experiments

A local increase in SIC surrounding the GrIS results in reduced evaporation over the North Atlantic ocean. This leads to a significant negative snowfall anomaly, mainly restricted to the south-eastern GrIS where precipitation peaks (Fig. 2 (a,b)). Snowfall anomalies at other locations are small and hence not visible in Fig. 2. No significant changes in rainfall, runoff and melting are simulated for a rise in SIC (Tab. 2). For the SIC +6 experiment, the wintertime near-surface air temperature decreases by about 10°C over the newly sea ice-covered areas, resulting from a substantial sensible heat flux reduction. In summer, the marginal sea ice and the surrounding SST are both close to the ice melting point (0°C), allowing no large change in near-surface air temperature above the ocean. Therefore, a sea ice increase in summer does not significantly impact GrIS runoff, since this ablation process is sensitive to positive anomalies in near-surface air temperature. This emphasizes that SIC operates as a heat and moisture insulator over the ocean, mainly affecting winter time sensible heat exchange and evaporation, whereas it presents a weak influence on summer near-surface air temperature, resulting in almost unchanged runoff over the GrIS (Fig. 3 (b,e)). As a result, the significant snowfall decrease in the south-eastern GrIS leads to a local significant negative anomaly in GrIS SMB (Fig. 5 (b)).

Conversely, a SIC retreat generates respectively a significant increase in snowfall over the south-east associated with scattered small drop in runoff. This ablation reduction might result from the local rise in summer snowfall (Tab. 2), enhancing the summer surface albedo and hence lowering the melt energy available at the surface. Both these processes imply a small but significant positive anomaly in SMB along the south-eastern GrIS coast (Fig. 5 (e)).

3.2 SST sensitivity experiments

Higher SST induces an increase in evaporation leading to significantly enhanced snowfall (Fig. 2 (f)) and rainfall (Fig. 4 (f)) over the south-eastern GrIS margins. In addition, positive SST anomalies partially convert summer snowfall into rainfall over this region (Tab. 2), wetting the snow cover and hence reducing the summer surface albedo. This increases the surface melting and runoff through the positive melt-albedo feedback. Similarly, a significant increase in runoff is simulated over the ablation zone in western Greenland, resulting from higher near-surface temperatures induced by the warmer surrounding ocean (Fig. 3 (f)).

Integrated over the GrIS, the local mass loss, induced by enhanced runoff in western Greenland, exceeds the south-east mass gain, resulting from increased precipitation (Tab. 2). This leads to a small but insignificant negative integrated SMB anomaly (Fig. 5 (f)). Opposite results are obtained for a reduction in SST (Fig. 5 (c)).

3.3 Combined SIC-SST sensitivity experiments

A combined decrease in SIC and rise in SST enhances significantly the positive snowfall anomaly relative to individual SIC or SST perturbations (Tab. 2 and Fig. 2 (g)), as both forcings favour increased evaporation above the northern Atlantic Ocean. Anomalies in rainfall and runoff (Fig. 4 and Fig. 3 (d,g)) are significant and similar to these induced by

an individual increase in SST (Fig. 4 and Fig. 3 (c,f)), since SIC perturbations have no significant influence on the summer near-surface air temperature. The decline in runoff is smaller for the SIC +6 / SST -4 experiment with respect to the SST -4 simulation (Tab. 2), because a SIC extension only generates significant negative snowfall anomalies. This results from the weakened SST influence on near-surface air temperature and hence on runoff when the sea ice expands. Likewise, the reduction in summer snowfall is similar to the SST +4 experiment, as SIC anomalies have no significant influence on summer snowfall (Tab. 2).

For a coupled increase in SIC and drop in SST, both the local mass loss, resulting from snowfall reduction in south-east Greenland, and the coastal mass gain due to decreased runoff are similar in magnitude and hence almost in balance when integrated over the whole GrIS (Fig. 5(d)). Opposite results are obtained for the SIC -6 / SST +4 experiment as displayed in Fig. 5(g). As a result, the local SMB anomalies induced by the combined forcing experiments are insignificant and smaller than those simulated in the individual sensitivity simulations (Tab. 2). This highlights the importance of accurately modelling the snowfall/runoff ratio as significant anomalies in these components tend to compensate each other, leaving the integrated SMB almost unchanged.

4 Discussion

None of the sensitivity experiments reveal a major direct SST or/and SIC impact on SMB when integrated over the GrIS for the 2007-2012 period (Tab. 2). The largest integrated SMB anomalies are $\pm$ 7% for the two most extreme SIC perturbations (Tab. 2). Compared to the 1979-2000 inter annual variability ($\approx$ 100 Gt/yr or $\approx$ 25%; Fettweis et al. (2013b)), these SMB anomalies are minor and fall within the MAR SMB uncertainty range of about $\pm$ 10% (Fettweis et al., 2013b). Although significant regional SMB anomalies exist in our sensitivity experiments, these are mostly restricted to the western coastal regions, driven by runoff perturbations, and the southeastern region, driven by snowfall changes (Fig. 5). As a result of unconsidered feedbacks on the general circulation, MAR suggests that integrated GrIS SMB varies linearly with individual perturbations in SIC and SST, whereas a nonlinear relationship is found for the combined SIC-SST forcings. This nonlinear relationship results from the compensating effect between ablation and accumulation anomalies when these are integrated over the ice sheet. Partly, these relationships between perturbed oceanic conditions and SMB might be attributed to the fixed atmospheric conditions prescribed in MAR, allowing for potentially different results if oceanic forcing feedbacks on the general circulation were taken into account.

4.1 Katabatic winds blocking effect

An important role in limiting the oceanic forcing impact on GrIS SMB is played by katabatic winds (Rennermalm et al., 2009). Katabatic winds result from negatively buoyant air over a sloping surface (Van Angelen et al., 2013), induced by a negative net surface energy budget, cooling the near-surface air temperature (Ettema et al., 2010). This leads to the formation of an anticyclonic circulation pattern centred over the GrIS, allowing cold and hence dense near-surface air to flow down from the GrIS summit towards the surrounding ocean by gravity (Heinemann, 1999).

As katabatic winds are directed offshore, they prevent near-surface oceanic moisture and temperature anomalies, induced by SIC or/and SST perturbations, from penetrating far onto the GrIS and hence from substantially affecting its SMB. Fig. 6 depicts the JJA mean anomalies in air temperature (°C), accounting for runoff perturbations, and the annual mean anomalies in specific humidity (g/kg), representative of the annual total accumulation, in the SIC -6 / SST +4 experiment. As the surface slope decreases over the tundra and surrounding oceans, katabatic winds cease, allowing a small oceanic influence on the SMB in low coastal regions. However, as humidity anomalies persist above the katabatic layer (Fig. 6), slightly enhanced moisture advection propagate towards the ice sheet interior in south-eastern Greenland, allowing local positive SMB anomalies to spread further inland. The western Greenland coast is more sensitive to oceanic forcing than the eastern coast (Fig. 6) partly due to its gentler slopes, leading to weaker katabatic winds. Since humidity and temperature perturbations are only restricted to the atmospheric boundary layer (Fig. 6), heat and moisture advection in the free atmosphere is not considerably affected by changes in near-surface air conditions over the ocean.

In agreement with Rennermalm et al. (2009), Ettema et al. (2010) and Van Angelen et al. (2013), oceanic forcing impact on GrIS SMB is enhanced in summer, when katabatic winds weaken (Fig. 6 (a)). This would be due to both an almost in balance net energy budget during summer (Ettema et al., 2010) as well as the resulting lower thermal gradient between the ice sheet interior and the surrounding ocean.

4.2 Oceanic forcing impacts on katabatic winds

Since sea ice does not substantially affect near-surface air temperature in summer, anomalies in SIC have no major impact on the JJA thermal gradient between the ice sheet and the ocean (Fig. 7 (b,e)), leading to negligible changes in katabatic wind intensity (Fig. 8 (b,e)). In winter, a SIC decrease results in a sharp rise in near-surface temperature, generating a slight surface pressure reduction over the oceanic areas affected by a sea ice retreat (Fig. 9 (e)). This leads to a small increase in the strength of winter katabatic flow (Fig. 10 (e)).

For higher SST, the horizontal temperature gradient increases with rising ocean temperatures (Fig. 7 and 9 (f)),

resulting in enhanced katabatic winds over coastal regions (Fig. 8 and Fig. 10 (f)). However, changes in surface conditions are less extensive in winter than in summer as the SST anomalies are restricted to ice-free oceanic areas. A considerable increase in katabatic wind intensity is thus limited to the summer season (Fig. 8 (f)).

Similar results are simulated for individual SST (Fig. 7 and Fig. 8 (c,f)) and combined SIC-SST anomalies in summer (Fig. 7 and Fig. 8 (d,g)) since summer SIC perturbations do not strongly affect near-surface air temperature. In winter, the combined effects of SIC retreat and SST increase on surface pressure add up to provide slightly stronger katabatic winds (Fig. 10 (d,g)).

5 Conclusions

The direct impact of oceanic forcing on GrIS SMB is limited to coastal regions, especially along the western periphery, where local SMB anomalies are induced by runoff perturbations, and the south-eastern coast, where SMB is driven by precipitation variability. Changes in SIC significantly affect winter snowfall in the south-eastern GrIS by modifying the moisture and heat fluxes between the ocean and the atmosphere. Solid precipitation is enhanced for a SIC retreat, leading to a significant positive anomaly in integrated GrIS SMB. An increase in SST also enhances evaporation and near-surface warming, leading to a rise in GrIS runoff which exceeds the increase in precipitation. When integrated over the whole ice sheet, the net result is an insignificant negative SMB anomaly. A combined SIC withdrawal associated with a SST increase, leads to both higher snowfall and runoff. Therefore, these ablation and accumulation processes compensate each other, leaving integrated SMB almost unchanged. These results are consistent with previous studies focusing on individual changes in SIC (Day et al., 2013), SST (Hanna et al., 2009), and combined SIC-SST forcings (Hanna et al., 2013a). However, Day et al. (2013) suggest a net decrease in integrated SMB induced by a SIC reduction combined with a SST increase. This contradictory result may be due to the fact that HadRM3 underestimates contemporary GrIS precipitation (Vernon et al., 2013) and the ITM SMB model overestimates runoff (Day et al., 2013). This stresses the importance of accurately modelling contemporary SMB components, since their response to combined oceanic forcings are non-linear as a result of the feedback between albedo, conditioned by snowfall anomalies, and surface melt.

This study underlines that direct oceanic forcing is very unlikely involved in the various melt records that were set over the GrIS since 2007. The main reason is that katabatic winds, flowing down the ice sheet slopes, are strong enough to prevent near-surface oceanic air from penetrating far onto the ice sheet and hence affecting its SMB. At most, oceanic forcing may have slightly contributed to local SMB anomalies in coastal regions, where katabatic winds dissipate. In a future warmer climate, a rise in SST associated with a decline in SIC might strengthen Greenland katabatic winds by enhancing the thermal contrast between the warmer ocean and the cold ice sheet interior. This might further reduce the direct oceanic impact on GrIS SMB.

The 2007-2012 melt records are thus more likely attributed to the recent persistent negative phase of the NAO, favouring anomalous south-westerly warm air advection towards the GrIS in the free atmosphere. Higher upper atmosphere temperatures would enhance the downward longwave radiation, warming up the GrIS surface and hence increasing the surface melting. Furthermore, oceanic forcing might have contributed indirectly to the recent negative NAO shift (Overland and Wang, 2010; Jaiser et al., 2012). Continued sea ice retreat in summer may thus lead to prolonged phases of negative NAO, further accelerating GrIS surface melt (Jaiser et al., 2012). By prescribing fixed annual mid-Pliocene Warm Period ($\approx$ 3 Ma) reconstructed SIC (i.e. sea ice-free Arctic Ocean in summer) and SST (i.e. 6 to 12°C warmer than present day) in the GENESIS 3.0 GCM, Koenig et al. (2014) revealed that a more permanent negative NAO pattern might occur in a similar future warmer climate. Considering this indirect oceanic forcing, their ice sheet model suggested that the latter general circulation perturbation might considerably affect the GrIS SMB and lead to both a reduced ice sheet extent ($\approx$ -71%) and volume ($\approx$ -83%), potentially resulting in a 5.8 m sea level rise. Therefore, the Arctic warming amplification, partly induced by the positive melt-albedo feedback, may also be a prime factor involved in the negative NAO trend observed since 2007 (Overland and Wang, 2010; Jaiser et al., 2012). Finally, even though direct oceanic forcing does not considerably and significantly affect GrIS SMB, it does substantially enhance the calving rate of marine terminating glaciers in the south-east and north-west of Greenland (Thomas et al., 2003; Howat et al., 2005; Luckman and Murray, 2005; Bindschadler, 2006), when warm North Atlantic water infiltrates coastal fjords and melts the bottom of floating glacier tongues (Hanna et al., 2009).

References

A. Arguez, J. J. O'Brien, and S. R. Smith. Air temperature impacts over eastern north america and europe associated with low-frequency north atlantic sst variability. *International Journal of Climatology*, 29:1 – 10, 2009. doi:10.1002/joc.1700.

J. L. Bamber, S. Ekholm, and W. B. Krabill. A new, high-resolution digital elevation model of greenland fully validated with airborne laser altimeter data. *Journal of Geophysical Research*, 106:6733 – 6745, 2001. doi:10.1029/2000JB900365.

J. L. Bamber, J. A. Griggs, R. T. W. L. Hurkmans, J. A. Dowdeswell, S. P. Gogineni, I. Howat, J. Mouginot, J. Paden, S. Palmer, E. Rignot, and D. Steinhage. A new bed elevation dataset for greenland. *The Cryosphere*, 7:499 – 510, 2013. doi:10.5194/tc-7-499-2013.

R. Bindschadler. Hitting the ice sheets where it hurts. *Science*, 311: 1720 – 1721, 2006. doi:10.1126/science.1125226.

J. E. Box, D. H. Bromwich, and L. S. Bai. Greenland ice sheet surface mass balance 1991-2000: application of polar mm5 mesoscale model and in situ data. *Journal of Geophysical Research*, 109, 2004. doi:10.1029/2003JD004451.

J. E. Box, X. Fettweis, d M. Tedesco J. C. Stroeve a, D. K. Hall, and K. Steffen. Greenland ice sheet albedo feedback: thermodynamics and atmospheric drivers. *The Cryosphere*, 6:821 – 839, 2012. doi:10.5194/tc-6-821-2012.

E. Brun, P. David, M. Sudul, and G. Brunot. A numerical model to simulate snow-cover stratigraphy for operational avalanche forecasting. *Journal of Glaciology*, 38:13 – 22, 1992.

E. Buch, S. A. Pedersen, and M. H. Ribergaard. Ecosystem variability in west greenland waters. *Journal of Northwest Atlantic Fishery Science*, 34:13 – 28, 2004. doi:10.2960/J.v34.m479.

J. C. Comiso, D. J. Cavalieri, C. L. Parkinson, and P. Gloersen. Passive microwave algorithms for sea ice concentration: a comparison of two techniques. *Remote Sensing of Environment*, 60:357 – 384, 1997. doi:http://dx.doi.org/10.1016/S0034-4257(96)00220-9.

J. C. Comiso, C. L. Parkinson, R. Gersten, and L. Stock. Accelerated decline in the arctic sea ice cover. *Geophysical Research Letters*, 35:6p., 2008. doi:10.1029/2007GL031972.

J. Day. *The impact of 21st century Arctic sea ice decline on the climate and mass balance of the Greenland ice sheet and Svalbard's glaciers and ice caps*. PhD thesis, University of Bristol, 2011.

J. J. Day, J. L. Bamber, and P. J. Valdes. The greenland ice sheet's surface mass balance in a seasonally sea ice-free arctic. *Journal of Geophysical Research: Earth Surface*, 118:1533 – 1544, 2013. doi:10.1002/jgrf.20112.

D. P. Dee, S. M. Uppala, A. J. Simmons, P. Berrisford, P. Poli, S. Kobayashi, U. Andrae, M. A. Balmaseda, G. Balsamo, P. Bauer, P. Bechtold, A. C. M. Beljaars, L. van de Berg, J. Bidlot, N. Bormann, C. Delsol, R. Dragani, M. Fuentes, A. J. Geer, L. Haimberger, S. B. Healy, H. Hersbach, E. V. Hólm, L. Isaksen, P. Kållberg, M. Köhler, M. Matricardi, A. P. McNally, B. M. Monge-Sanz, J.-J. Morcrette, B.-K. Park, C. Peubey, P. de Rosnay, C. Tavolato, J.-N. Thépaut, and F. Vitart. The era-interim reanalysis: configuration and performance of the data assimilation system. *Quarterly Journal of the Royal Meteorological Society*, 137:553 – 597, 2011. doi:10.1002/qj.828.

C. Deser, J. E. Walsh, and M. S. Tilmin. Arctic sea ice variability in the context of recent atmospheric circulation trends. *Journal of Climate*, 13: 617 – 633, 2000. doi:http://dx.doi.org/10.1175/1520-0442(2000)013<0617:ASIVIT>2.0.CO;2.

H. A. Dijkstra, L. te Raa, M. Schmeits, and J. Gerrits. On the physics of the atlantic multidecadal oscillation. *Ocean Dynamics*, 56:36 – 50, 2006. doi:10.1007/s10236-005-0043-0.

E. M. Enderlin and I. M. Howat. Submarine melt rate estimates for floating termini of greenland outlet glaciers (2000–2010). *Journal of Glaciology*, 59:67 – 75, 2013. doi:10.3189/2013JoG12J049.

D. B. Enfield, A. M. Mestas-Nuñez, and P. J. Trimble. The atlantic multidecadal oscillation and its relation to rainfall and river flows in the continental u.s. *Geophysical Research Letters*, 28:2077 – 2080, 2001. doi:10.1029/2000GL012745.

J. Ettema, M. R. van den Broeke, E. van Meijgaard, and W. J. van de Berg. Climate of the greenland ice sheet using a high-resolution climate model - part2: Near-surface climate and energy balance. *The Cryosphere*, 4:529 – 544, 2010. doi:10.5194/tc-4-529-2010.

X. Fettweis. Reconstruction of the 1979-2006 greenland ice sheet surface mass balance using the regional climate model mar. *The Cryosphere*, 1:21 – 40, 2007. doi:10.5194/tc-1-21-2007.

X. Fettweis, H. Gallée, F. Lefebre, and J.-P. van Ypersele. Greenland surface mass balance simulated by a regional climate model and comparison with satellite-derived data in 1990-1991. *Climate Dynamics*, 24:623 – 640, 2005. doi:10.1007/s00382-005-0010-y.

X. Fettweis, M. Tedesco, M. van den Broeke, and J. Ettema. Melting trends over the greenland ice sheet (1958-2009) from spaceborne microwave data and regional climate models. *The Cryosphere*, 5: 359 – 375, 2011. doi:10.5194/tc-5-359-2011.

X. Fettweis, B. Franco, M. Tedesco, J. H. van Angelen, J. T. M. Lenaerts, M. R. van den Broeke, and H. Gallée. Estimating the greenland ice sheet surface mass balance contribution to future sea level rise using the regional atmospheric climate model mar. *The Cryosphere*, 7:469 – 489, 2013a. doi:10.5194/tc-7-469-2013.

X. Fettweis, E. Hanna, C. Lang, A. Belleflamme, M. Erpicum, and H. Gallée. Brief communication: Important role of the mid-tropospheric atmospheric circulation in the recent surface melt increase over the greenland ice sheet. *The Cryosphere*, 7:241 – 248, 2013b. doi:10.5194/tc-7-241-2013.

C. G. Fletcher. *Investigations into Seasonal Predictability of North Atlantic Winter Climate*. PhD thesis, University of London, 2005.

B. Franco, , X. Fettweis, M. Erpicum, and S. Nicolay. Present and future climates of the greenland ice sheet according to the ipcc ar4 models. *Climate Dynamics*, 36:1897 – 1918, 2011. doi:10.1007/s00382-010-0779-1.

B. Franco, X. Fettweis, C. Lang, and M. Erpicum. Impact of spatial resolution on the modelling of the greenland ice sheet surface mass balance between 1990–2010, using the regional climate model mar. *The Cryosphere*, 6:695 – 711, 2012. doi:10.5194/tc-6-695-2012.

H. Gallée and G. Schayes. Development of a three-dimensional meso-γ primitive equation model: Katabatic winds simulation in the area of terra nova bay, antarctica. *Monthly Weather Review*, 122:671 – 685, 1994. doi:http://dx.doi.org/10.1175/1520-0493(1994)122<0671:DOATDM>2.0.CO;2.

H. Gallée, G. Guyomarc'h, and E. Brun. Impact of snow drift on the antarctic ice sheet surface mass balance: possible sensitivity to snow-surface properties. *Boundary-Layer Meteorology*, 99:1 – 19, 2001.

H. Gallée, V. Peyaud, and I. Goodwin. Simulation of the net snow accumulation along the wilkes land transect, antarctica, with a regional climate model. *Annals of Glaciology*, 41:17 – 22, 2005. doi:http://dx.doi.org/10.3189/172756405781813230.

R. G. Graversen, T. Mauritsen, M. Tjernstrom, E. Kallen, and G. Svensson. Vertical structure of recent arctic warming. *Nature*, 451:53 – 56, 2008. doi:10.1038/nature06502.

E. Hanna and J. Cappelen. Recent cooling in coastal southern greenland and relation with the north atlantic oscillation. *Geophysical Research Letters*, 30, 2003. doi:10.1029/2002GL015797.

E. Hanna, J. Cappelen, X. Fettweis, P. Huybrechts, A. Luckman, and M. H. Ribergaard. Hydrologic response of the greenland

ice sheet: the role of oceanographic warming. *Hydrological Processes*, 23:7 – 30, 2009. doi:10.1002/hyp.7090.

E. Hanna, X. Fettweis, S. H. Mernild, J. Cappelen, M. H. Ribergaard, C. Shuman, K. Steffen, L. Wood, and T. L. Mote. Atmospheric and oceanic climate forcing of the exceptional greenland ice sheet surface melt in summer 2012. *Journal of Climatology*, 2013a. doi:10.1002/joc.3743.

E. Hanna, J. M. Jones, J. Cappelen, S. H. Mernild, L. Wood, K. Steffen, and P. Huybrechts. The influence of north atlantic atmospheric and oceanic forcing effects on 1900-2010 greenland summer climate and ice melt/runoff. *International Journal of Climatology*, 33:862 – 880, 2013b. doi:10.1002/joc.3475.

G. Heinemann. The kabeg'97 field experiment: an aircraft-based study of katabatic wind dynamics over the greenland ice sheet. *Boundary Layer Meteorology*, 93:75 – 116, 1999.

B. J. Hoskins and K. I. Hodges. New perspectives on the northern hemisphere winter storm track. *Journal of the Atmospheric Sciences*, 59:1041 – 1061, 2002. doi:http://dx.doi.org/10.1175/1520-0469(2002)059<1041:NPOTNH>2.0.CO;2.

I. M. Howat, I. Joughin, S. Tulaczyk, and S. Gogineni. Rapid retreat and acceleration of helheim glacier, east greenland. *Geophysical Research Letters*, 32, 2005. doi:10.1029/2005GL024737.

I. M. Howat, I. Joughin, M. Fahnestock, B. E. Smith, and T. A. Scambos. Synchronous retreat and acceleration of southeast greenland outlet glaciers 2000-2006: Ice dynamics and coupling to climate. *Journal of Glaciology*, 54:646 – 660, 2008.

R. Jaiser, K. Dethloff, D. Handorf, A. Rinke, and J. Cohen. Impact of sea ice cover changes on the northern hemisphere atmospheric winter circulation. *Tellus*, 64:11 p., 2012. doi:10.3402/tellusa.v64i0.11595.

P. D. Jones, T. Jonsson, and D. Wheeler. Extension to the north atlantic oscillation using early instrumental pressure observations from gibraltar and south-west iceland. *International Journal of Climatology*, 17:1433 – 1450, 1997. doi:10.1002/(SICI)1097-0088(19971115)17:13<1433::AID-JOC203>3.0.CO;2-P.

S. J. Koenig, R. M. DeConto, and D. Pollard. Impact of reduced arctic sea ice on greenland ice sheet variability in a warmer than present climate. *Geophysical Research Letters*, 2014. doi:10.1002/2014GL059770.

W. Krabill, E. Frederick, S. Manizade, C. Martin, J. Sonntag, R. Swift, R. Thomas, W. Wright, and J. Yungel. Rapid thinning of parts of the southern greenland ice sheet. *Science*, 283:1522 – 1524, 1999. doi:10.1126/science.283.5407.1522.

F. Lefebre, H. Gallée, J.-P. van Ypersele, and W. Greuell. Modeling of snow and ice melt at eth camp (west greenland): a study of surface albedo. *Journal of Geophysical Research*, 108, 2003. doi:10.1029/2001JD001160.

F. Lefebre, X. Fettweis, H. Gallée, J.-P. van Ypersele P. Marbaix, W. Greuell, and P. Calanca. Evaluation of a high-resolution regional climate simulation over greenland. *Climate Dynamics*, 25: 99 – 116, 2005. doi:10.1007/s00382-005-0005-8.

J. T. M. Lenaerts, M. R. van den Broeke, J. H. Angelen, E. van Meijgaard, and S. J. Déry. Drifting snow climate of the greenland ice sheet: a study with a regional climate model. *The Cryosphere Discussion*, 6:1611 – 1635, 2012. doi:10.5194/tcd-6-1611-2012.

A. Luckman and T. Murray. Seasonal variation in velocity before retreat of jakobshavn isbrae, greenland. *Geophysical Research Letters*, 32, 2005. doi:10.1029/2005GL022519.

S. H. Mernild, G. E. Liston, C. A. Hiemstra, and J. H. Christensen. Greenland ice sheet surface mass-balance modeling in a 131-yr perspective, 1950-2080. *Journal of Hydrometeorology*, 11:3 – 25, 2010. doi:10.1175/2009JHM1140.1.

S. H. Mernild, T. L. Mote, and G. E. Liston. Greenland ice sheet surface melt extent and trends: 1960-2011. *Journal of Glaciology*, 57:621 – 628, 2011.

T. L. Mote. Mid-tropospheric circulation and surface melt on the greenland ice sheet. part i: Atmospheric teleconnections. *International Journal of Climatology*, 18:111 – 129, 1998. doi:10.1002/(SICI)1097-0088(199802)18:2<111::AID-JOC227>3.0.CO;2-X.

T. J. Osborn. Simulating the winter north atlantic oscillation: the roles of internal variability and greenhouse gas forcing. *Climate Dynamics*, 22:605 – 623, 2004. doi:10.1007/s00382-004-0405-1.

J. E. Overland and M. Wang. Large-scale atmospheric circulation changes are associated with the recent loss of arctic sea ice. *Tellus*, 62:1 – 9, 2010. doi:10.1111/j.1600-0870.2009.00421.x.

J. E. Overland, J. A. Francis, E. Hanna, and M. Wang. The recent shift in early summer arctic atmospheric circulation. *Geophysical Research Letters*, 39:L19804, 2012. doi:10.1029/2012GL053268.

A. K. Rennermalm, L. C. Smith, J. C. Stroeve, and V. W. Chu. Does sea ice influence greenland ice sheet surface-melt ? *Environmental Research Letters*, 4:6p., 2009. doi:10.1088/1748-9326/4/2/024011.

K. De Ridder and H. Gallée. Land surface-induced regional climate change in southern israel. *Journal of Applied Meteorology*, 37:1470 – 1485, 1998. doi:http://dx.doi.org/10.1175/1520-0450(1998)037<1470:LSIRCC>2.0.CO;2.

E. Rignot, I. Velicogna, M. R. van den Broeke, A. Monaghan, and J. Lenaerts. Acceleration of the contribution of the greenland and antarctic ice. *Geophysical Research Letters*, 38:L05503/1 – L05503/5, 2011. doi:10.1029/2011GL046583.

I. G. Rigor, J. M. Wallace, and R. L. Colony. Response of sea ice to the arctic oscillation. *Journal of Climate*, 15:2648 – 2663, 2002. doi:http://dx.doi.org/10.1175/1520-0442(2002)015<2648:ROSITT>2.0.CO;2.

M. C. Serreze, M. M. Holland, and J. Stroeve. Perspectives on the arctic's shrinking sea-ice cover. *Science*, 315:1533 – 1536, 2007. doi:10.1126/science.1139426.

A. Shepherd, E. R. Ivins, G. A, V. R. Barletta, M. J. Bentley, S. Bettadpur, K. H. Briggs, D. H. Bromwich, R. Forsberg, N. Galin, M. Horwath, S. Jacobs, I. Joughin, M. A. King, J. T. M. Lenaerts, J. Li, S. R. M. Ligtenberg, A. Luckman, S. B. Luthcke, M. McMillan, R. Meister, G. Milne, J. Mouginot, A. Muir, J. P. Nicolas, J. Paden, A. J. Payne, H. Pritchard, E. Rignot, H. Rott, L. Sandberg Sørensen, T. A. Scambos, B. Scheuchl, E. J. O. Schrama, B. Smith, A. V. Sundal, J. H. van Angelen, W. J. van de Berg, M. R. van den Broeke, D. G. Vaughan, I. Velicogna, J. Wahr, P. L. Whitehouse, D. J. Wingham, D. Yi, D. Young, and H. J. Zwally. A reconciled estimate of ice-sheet mass balance. *Science*, 338:1183 – 1189, 2012. doi:10.1126/science.1228102.

S. Solomon, D. Qin, M. Manning, R. B. Alley, T. Berntsen, N. L. Bindoff, Z. Chen, A. Chidthaisong, J. M. Gregory, G. C. Hegerl, M. Heimann, B. Hewitson, B. J. Hoskins, F. Joos, J. Jouzel, V. Kattsov, U. Lohmann, T. Matsuno, M. Molina, N. Nicholls-sand J. Overpeck, G. Raga, V. Ramaswamy, J. Ren, M. Rustic-

ucci, R. Somerville, T. F. Stocker, P. Whetton, R. A. Wood, and D. Wratt. *Technical Summary, in: Climate Change 2007: The Physical Science Basis, Contribution of Working Group I to the Fourth Assessment Report of the Intergovernmental Panel on Climate Change*. Cambridge University Press, Cambridge, United Kingdom and New York, NY, USA, 2007.

J. D. Stark, Exeter Met Office, C. J. Donlon, M. J. Martin, and M. E. McCulloch. Ostia: An operational, high resolution, real time, global sea surface temperature analysis system. *OCEANS 2007 - Europe*, pages 1 – 4, 2007. doi:10.1109/OCEANSE.2007.4302251. Conference Publications.

J. C. Stroeve, M. C. Serreze, M. M. Holland, J. E. Kay, J. Malanik, and A. P. Barret. The arctic's rapidly shrinking sea ice cover: a research synthesis. *Climatic Change*, 110:1005 – 1027, 2012. doi:10.1007/s10584-011-0101-1.

R. T. Sutton and D. L. R. Hodson. Atlantic ocean forcing of north american and european summer climate. *Science*, 309:115 – 118, 2005. doi:10.1126/science.1109496.

M. Tedesco and X. Fettweis. 21st century projections of surface mass balance changes for major drainage systems of the greenland ice sheet. *Environmental Research Letters*, 7:11p., 2012. doi:10.1088/1748-9326/7/4/045405.

M. Tedesco, M. Serreze, and X. Fettweis. Diagnosing the extreme surface melt event over southwestern greenland in 2007. *The Cryosphere*, 2:159 – 166, 2008. doi:10.5194/tc-2-159-2008.

M. Tedesco, X. Fettweis, T. Mote, J. Wahr, P. Alexander, J. E. Box, and B. Wouters. Evidence and analysis of 2012 greenland records from spaceborne observations, a regional climate model and reanalysis data. *The Cryosphere*, 7:615 – 630, 2013. ISSN 1994 - 0416. doi:10.5194/tc-7-615-2013.

R. H. Thomas, W. Abdalati, E. Frederick, W. B. Krabill, S. Manizade, and K. Steffen. Investigation of surface melting and dynamic thinning on jakobshavn isbrae, greenland. *Journal of Glaciology*, 49:231 – 239, 2003. doi:http://dx.doi.org/10.3189/172756503781830764.

D. W. J. Thompson and J. M. Wallace. The arctic oscillation signature in the wintertime geopotential height and temperature fields. *Geophysical Research Letters*, 25:1297 – 1300, 1998. doi:10.1029/98GL00950.

J. H. Van Angelen, M. R. van den Broeke, B. Wouters, and J. T. M. Lenaerts. Contemporary (1969-2012) evolution of the climate and surface mass balance of the greenland ice sheet. *Surveys in Geophysics*, 2013. doi:10.1007/s10712-013-9261-z.

M. Van den Broeke, J. Bamber, J. Ettema, E. Rignot, E. Schrama, W. J. van de Berg, E. van Meijgaard, I. Velicogna, and B. Wouters. Partitioning recent greenland mass loss. *Science*, 326:984 – 986, 2009. doi:10.1126/science.1178176.

S. A. Venegas and L. A. Mysak. Is there a dominant timescale of natural climate variability in the arctic ? *Journal of Climate*, 13:3412 – 3434, 2000. doi:http://dx.doi.org/10.1175/1520-0442(2000)013<3412:ITADTO>2.0.CO;2.

C. L. Vernon, J. L. Bamber, J. E. Box, M. R. van den Broeke, X. Fettweis, E. Hanna, and P. Huybrechts. Surface mass balance model intercomparison for the greenland ice sheet. *The Cryosphere*, 7: 599 – 614, 2013. doi:10.5194/tc-7-599-2013.

B. Wouters, J. L. Bamber, M. R. van den Broeke, J. T. M. Lenaerts, and I. Sasgen. Limits in detecting acceleration of ice sheet mass loss due to climate variability. *Nature Geoscience*, 6:613 – 616, 2013. doi:10.1038/ngeo1874.

Period	Run	JJA SIC (10^6 km^2)		JJA SST (°C)	
		Mean	Anomaly	Mean	Anomaly
1979-2000	Observed	2.54	-	10.29	-
2001-2012	Observed	2.42	-0.11	11.07	0.78
2007-2012	Observed	2.29	-0.25	11.17	0.88
2007-2012	SIC +6	3.58	1.04	11.17	0.88
2007-2012	SIC +3	3.00	0.46	11.17	0.88
2007-2012	SIC -3	1.65	-0.89	11.17	0.88
2007-2012	SIC -6	1.21	-1.32	11.17	0.88
2007-2012	SST -4	2.29	-0.25	7.17	-2.12
2007-2012	SST -2	2.29	-0.25	9.17	-1.12
2007-2012	SST +2	2.29	-0.25	13.17	2.88
2007-2012	SST +4	2.29	-0.25	15.17	4.88

Table 1. Observed and applied JJA SIC and SST within MAR domain. The SST is calculated for the assumed sea ice-free ocean only (SIC ≤ 0.2) using the region within the black box displayed in Figure 1.

Mean (Gt yr^{-1})	**SMB**	**SMB %**	**Snowfall**	**Rainfall**	**Runoff**	**Melting**	**JJA SF**
Reference	237	-	555	28	354	585	117
Anomaly (Gt yr^{-1})	**SMB**	**SMB %**	**Snowfall**	**Rainfall**	**Runoff**	**Melting**	**JJA SF**
SIC +3	**-8**	-3.4	**-7**	0	1	1	1
SIC +6	**-15**	-6.3	**-16**	**-1**	-1	-1	2
SIC -3	**10**	+4.2	**9**	0	**-2**	-2	1
SIC -6	**16**	+6.8	**13**	0	**-3**	**-4**	2
SST -2	8	+3.4	**-7**	**-2**	**-17**	**-13**	**5**
SST -4	15	+6.3	**-12**	**-4**	**-29**	**-22**	**8**
SST +2	-5	-2.1	**17**	**4**	**25**	**23**	**-4**
SST +4	-13	-5.5	**37**	**9**	**59**	**54**	**-9**
SIC +3 / SST -2	-1	-0.4	**-14**	**-2**	**-14**	**-10**	**4**
SIC +6 / SST -4	2	+0.8	**-19**	**-4**	**-22**	**-15**	**7**
SIC -3 / SST +2	1	+0.4	**23**	**4**	**26**	**24**	**-4**
SIC -6 / SST +4	-7	-3	**48**	**10**	**64**	**58**	**-10**

Table 2. Top: annual mean cumulated GrIS SMB (Gt yr^{-1}) and its components (Gt yr^{-1}) for the reference run (2007–2012). Bottom: difference in SMB (Gt yr^{-1} and %) and its components (Gt yr^{-1}) between each sensitivity experiment and the reference run over 2007–2012. The last column lists JJA mean cumulated snowfall (Gt/JJA) over the GrIS for the reference run (top) and the anomalies (Gt/JJA) induced by each sensitivity experiment (bottom). Significant anomalies are displayed in bold for each experiment.

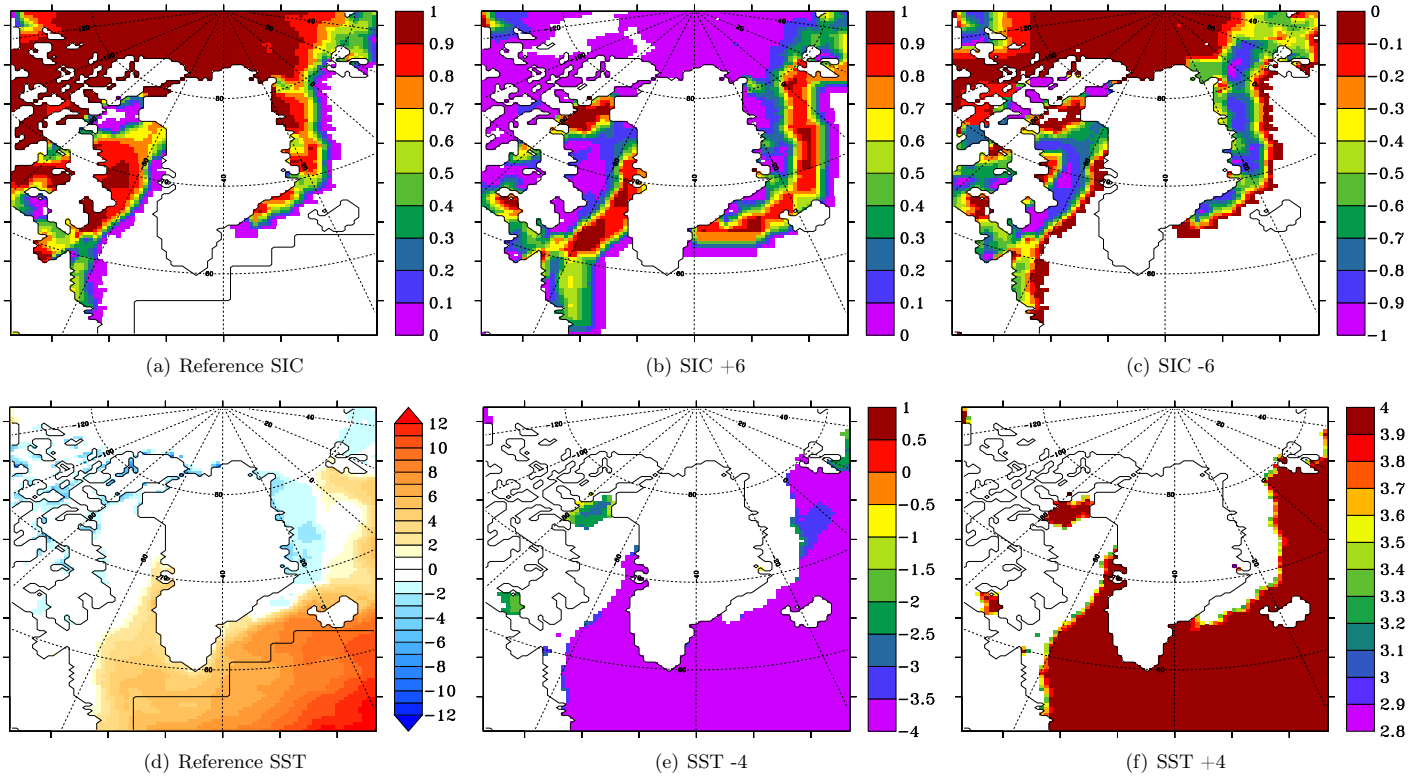

Fig. 1. Panel representing the entire integration domain used for every simulations. Top: reference simulation (a) SIC (% normalised to 1) and anomalies in SIC from the sensitivity experiment (b) SIC +6, (c) SIC -6 on the 1^{st} of June 2012. Bottom: reference simulation (d) SST (ºC) and anomalies in SST from the sensitivity experiment (e) SST -4, (f) SST +4 on the 1^{st} of June 2012. The black box area depicted in (a) and (d) is used to calculate SST in Tab. 1.

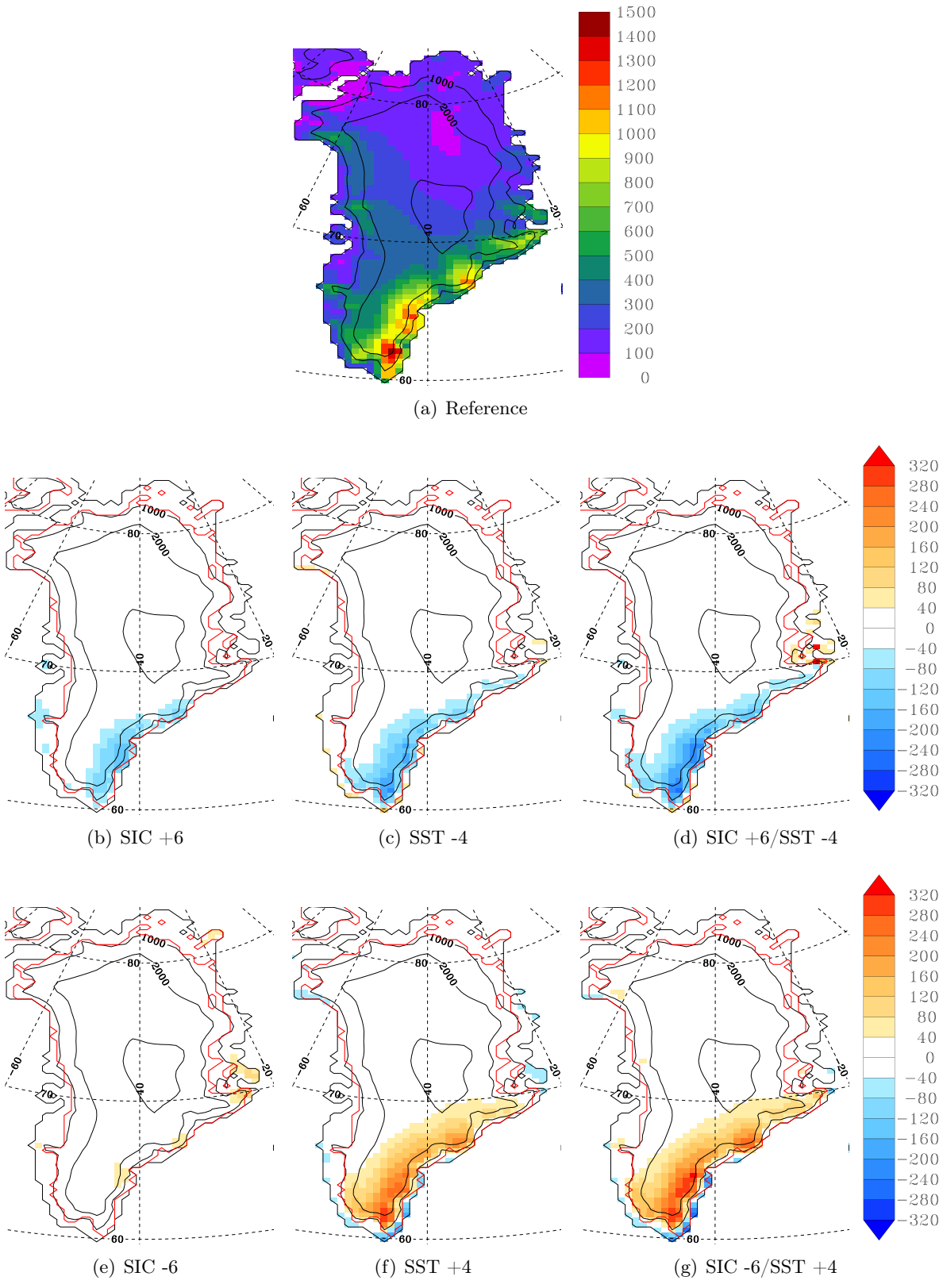

(a) Reference

(b) SIC +6

(c) SST -4

(d) SIC +6/SST -4

(e) SIC -6

(f) SST +4

(g) SIC -6/SST +4

Fig. 2. Annual mean cumulated snowfall (mmWE yr^{-1}) for the reference run (a), using the MAR model over 2007–2012. Difference in annual mean cumulated snowfall (mmWE yr^{-1}) between (b) SIC +6, (c) SST -4, (d) SIC +6 / SST -4, (e) SIC -6, (f) SST +4, (g) SIC -6 / SST +4 experiments and the reference run. The red thick line defines the GrIS area in MAR.

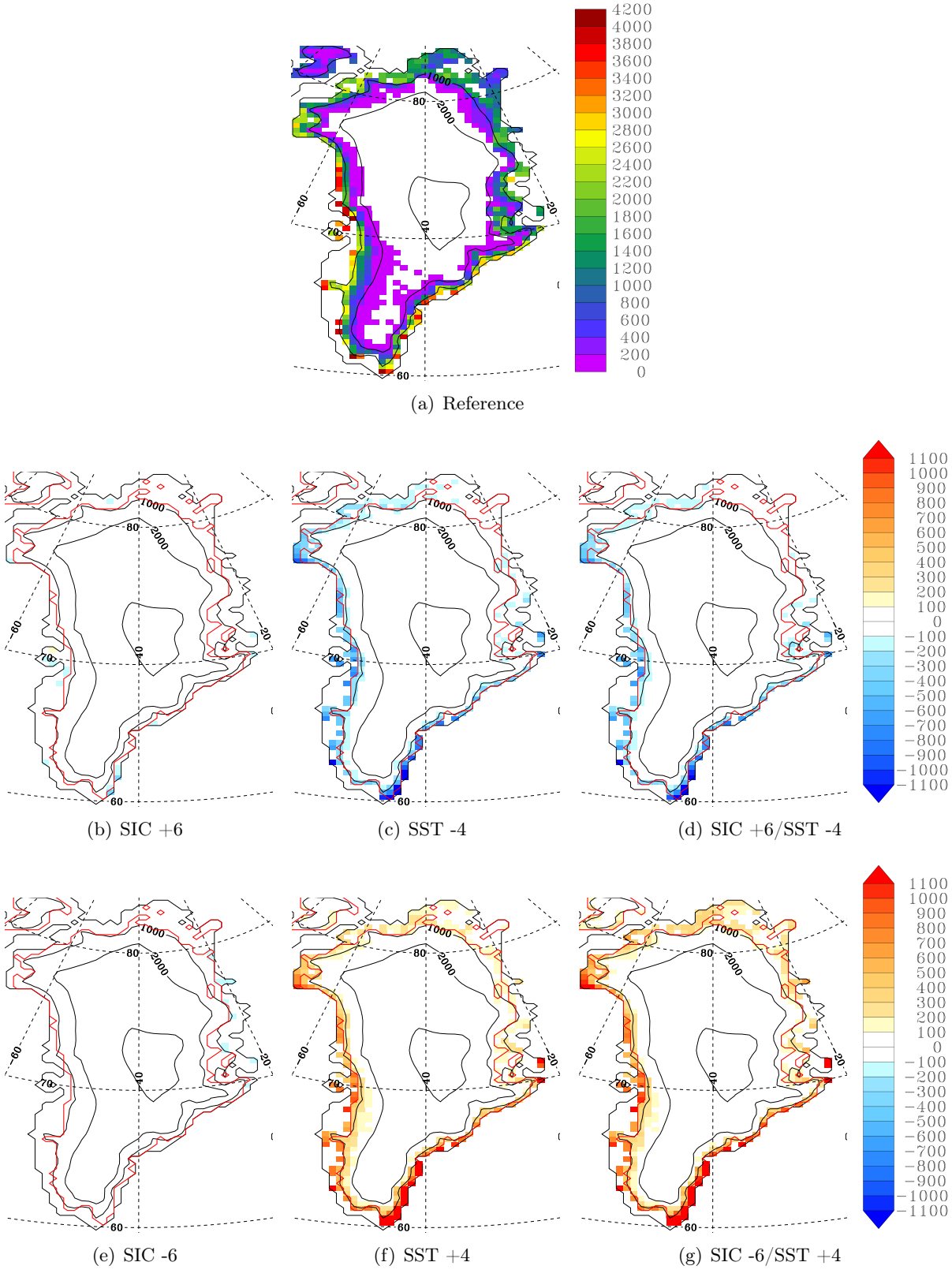

(a) Reference

(b) SIC +6

(c) SST -4

(d) SIC +6/SST -4

(e) SIC -6

(f) SST +4

(g) SIC -6/SST +4

Fig. 3. Annual mean cumulated runoff (mmWE yr^{-1}) for the reference run (a) over 2007–2012. Difference in annual mean cumulated runoff (mmWE yr^{-1}) between (b) SST -4, (c) SIC +6 / SST -4, (d) SST +4, (e) SIC -6 / SST +4 experiments and the reference run. The red thick line defines the GrIS area in MAR.

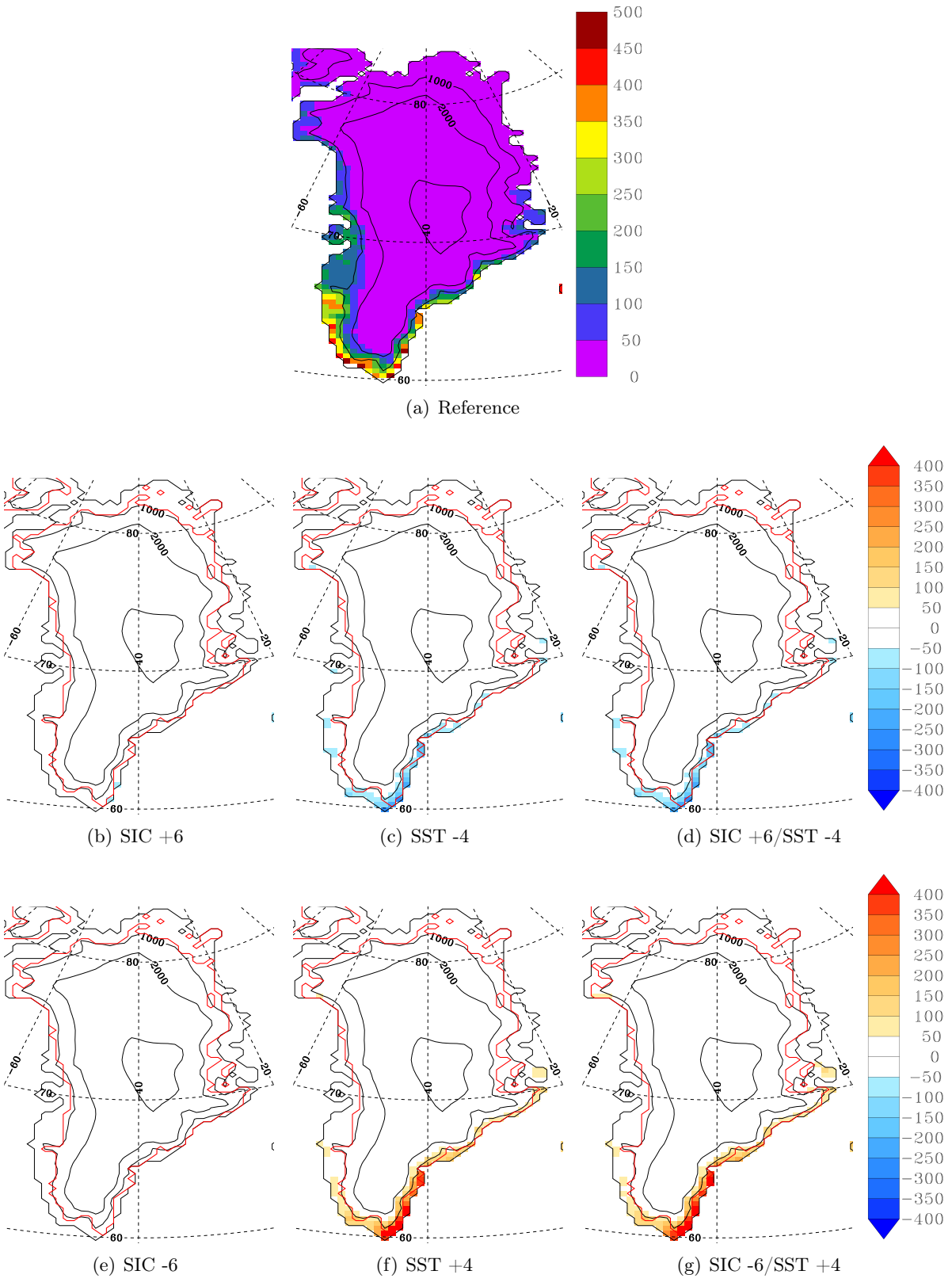

(a) Reference

(b) SIC +6

(c) SST -4

(d) SIC +6/SST -4

(e) SIC -6

(f) SST +4

(g) SIC -6/SST +4

Fig. 4. Annual mean cumulated rainfall (mmWE yr^{-1}) for the reference run (a) over 2007–2012. Difference in annual mean cumulated rainfall (mmWE yr^{-1}) between (b) SST -4, (c) SIC +6 / SST -4, (d) SST +4, (e) SIC -6 / SST +4 experiments and the reference run. The red thick line defines the GrIS area in MAR.

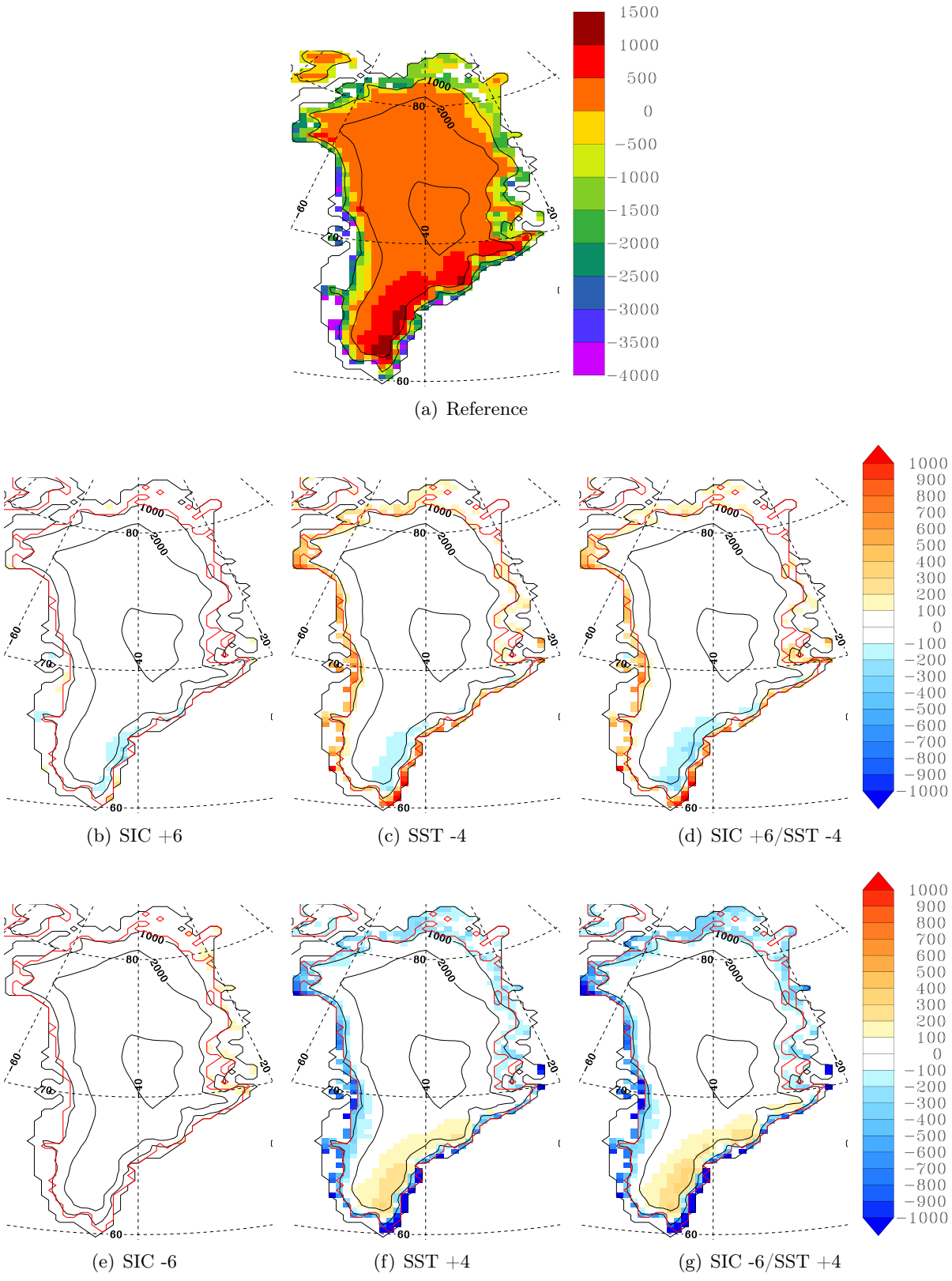

(a) Reference

(b) SIC +6

(c) SST -4

(d) SIC +6/SST -4

(e) SIC -6

(f) SST +4

(g) SIC -6/SST +4

Fig. 5. Annual mean cumulated SMB (mmWE yr^{-1}) for the reference run (a), using the MAR model (2007–2012). Difference in the annual mean cumulated SMB (mmWE yr^{-1}) between (b) SIC +6, (c) SST -4, (d) SIC +6 / SST -4, (e) SIC -6, (f) SST +4, (g) SIC -6 / SST +4 experiments and the reference run.The red thick line defines the GrIS area in MAR.

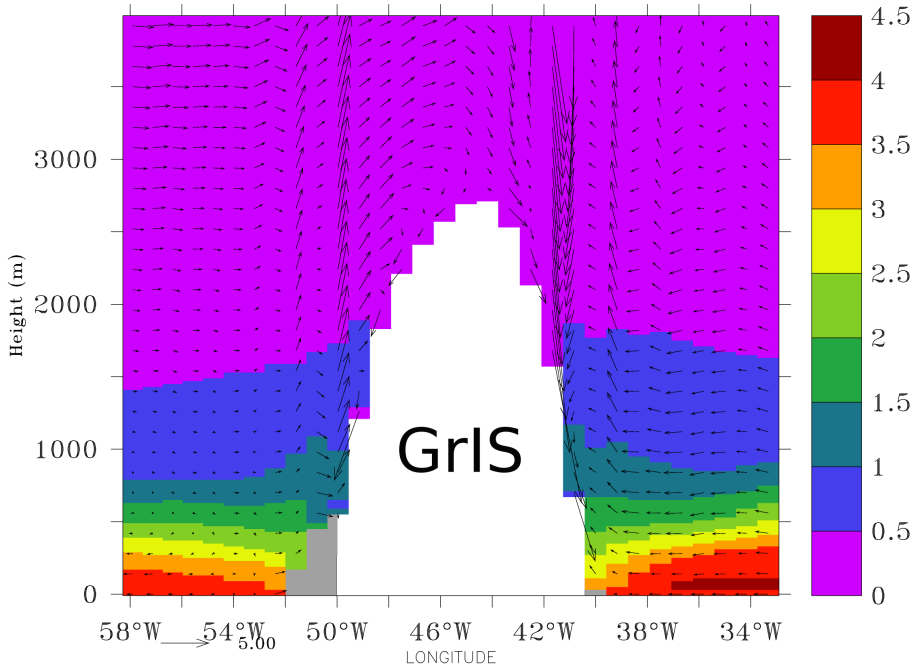

(a) JJA mean air temperature anomaly (°C)

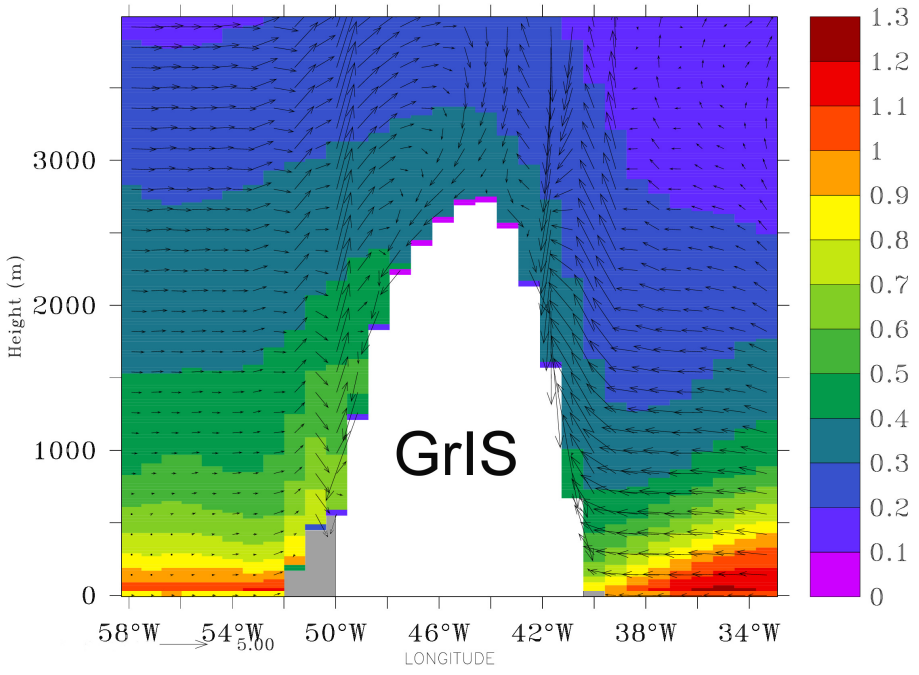

(b) Annual mean specific humidity anomaly (g/kg)

Fig. 6. Longitudinal section trough the GrIS (60°N), showing in the background (a) the difference between JJA mean air temperature (°C) from the SIC -6 / SST +4 and the reference run, (b) same for annual mean specific humidity (g/kg). The overlayed vectors represent (a) JJA mean wind speed (m/s) for the reference run over 2007–2012, (b) same for annual mean. The wind speed can be estimated using the arrow size (5 m/s) beneath the graphs. The grey area corresponds to the tundra region surrounding the GrIS.

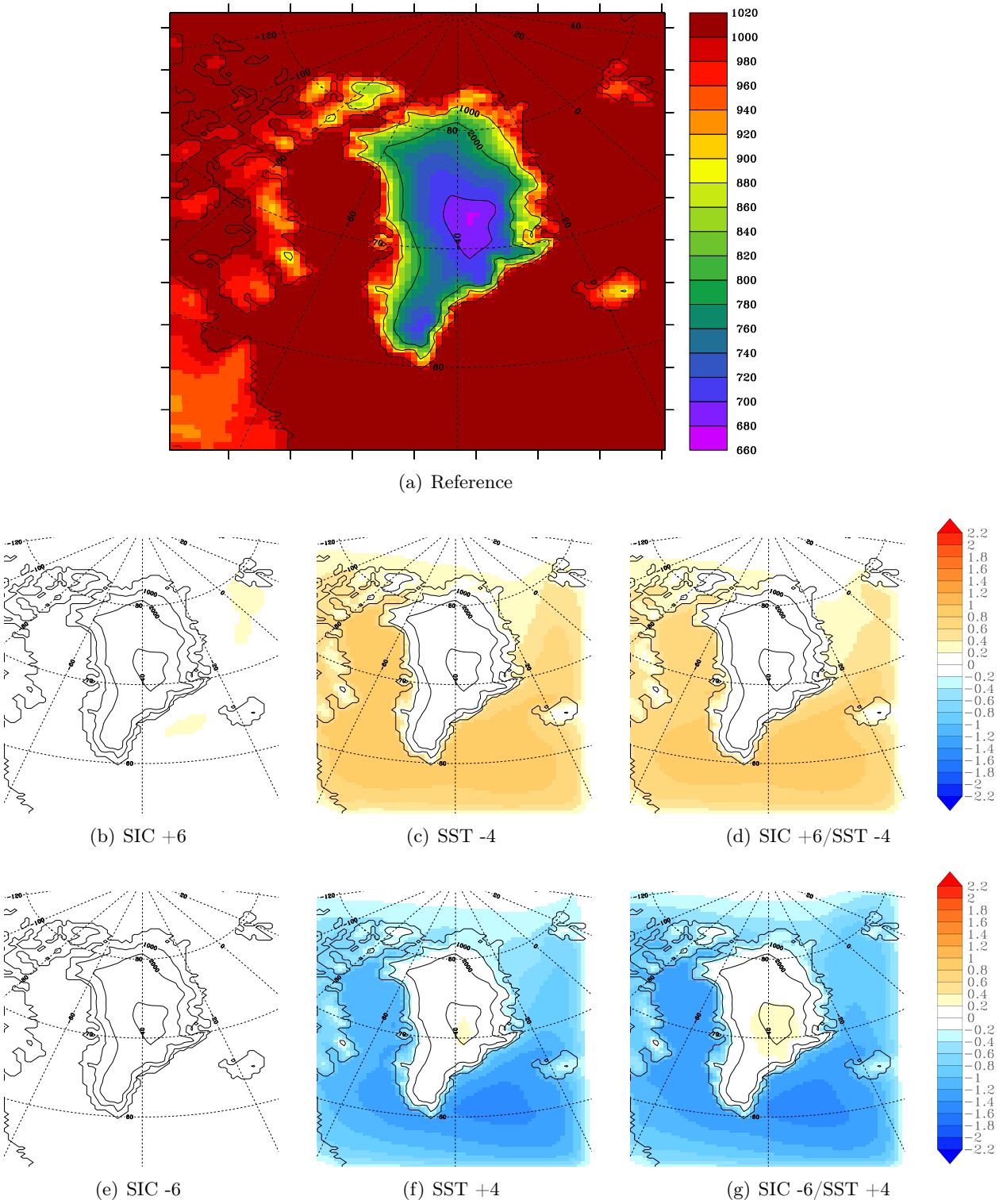

(a) Reference

(b) SIC +6

(c) SST -4

(d) SIC +6/SST -4

(e) SIC -6

(f) SST +4

(g) SIC -6/SST +4

Fig. 7. JJA mean surface pressure (hPa) for the reference run (a) over 2007–2012. Difference in JJA mean surface pressure (hPa) between (b) SIC +6, (c) SST -4, (d) SIC +6/SST -4, (e) SIC -6, (f) SST +4, (g) SIC -6 / SST +4 experiments and the reference run.

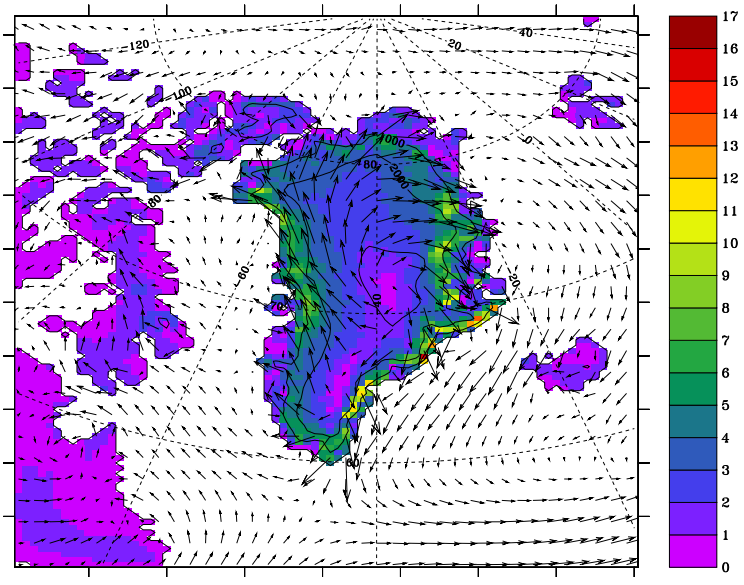

(a) Reference

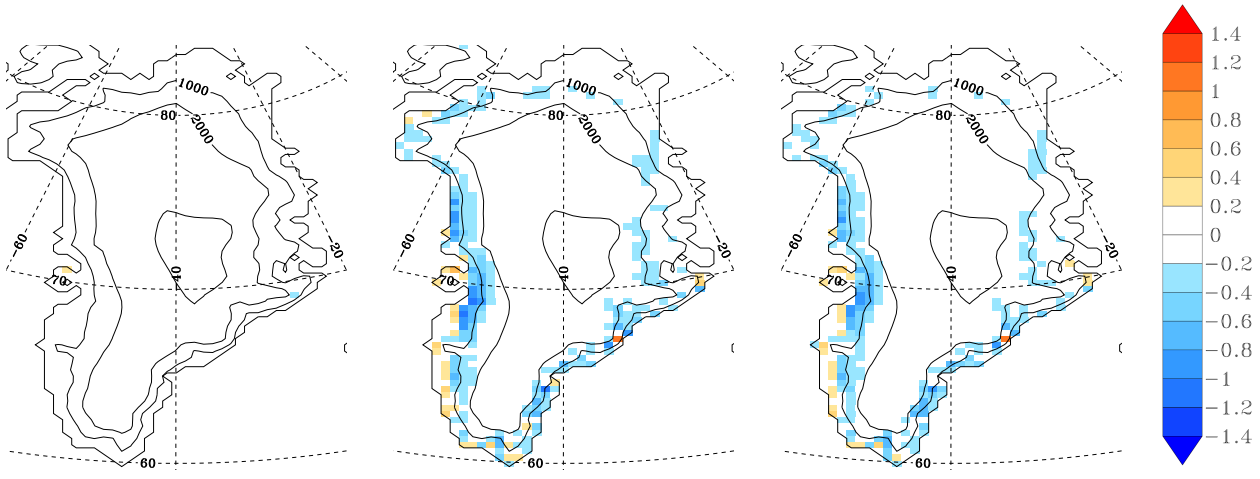

(b) SIC +6 (c) SST -4 (d) SIC +6/SST -4

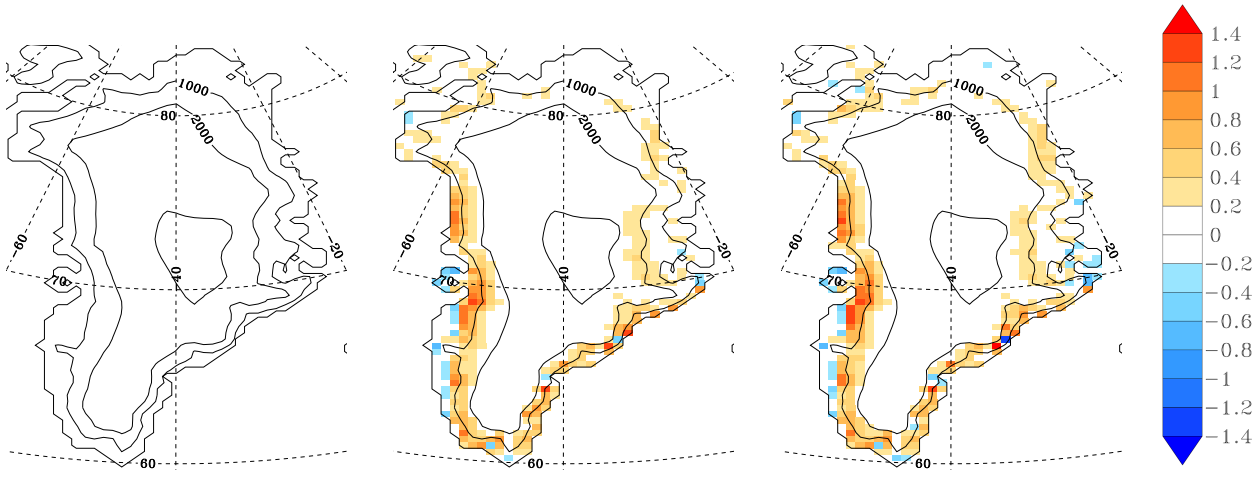

(e) SIC -6 (f) SST +4 (g) SIC -6/SST +4

Fig. 8. JJA mean wind speed (m/s) for the reference run (a) over 2007–2012. Difference in the JJA mean wind speed (m/s) between (b) SIC +6, (c) SST -4, (d) SIC +6/SST -4, (e) SIC -6, (f) SST +4, (g) SIC -6 / SST +4 experiments and the reference run.

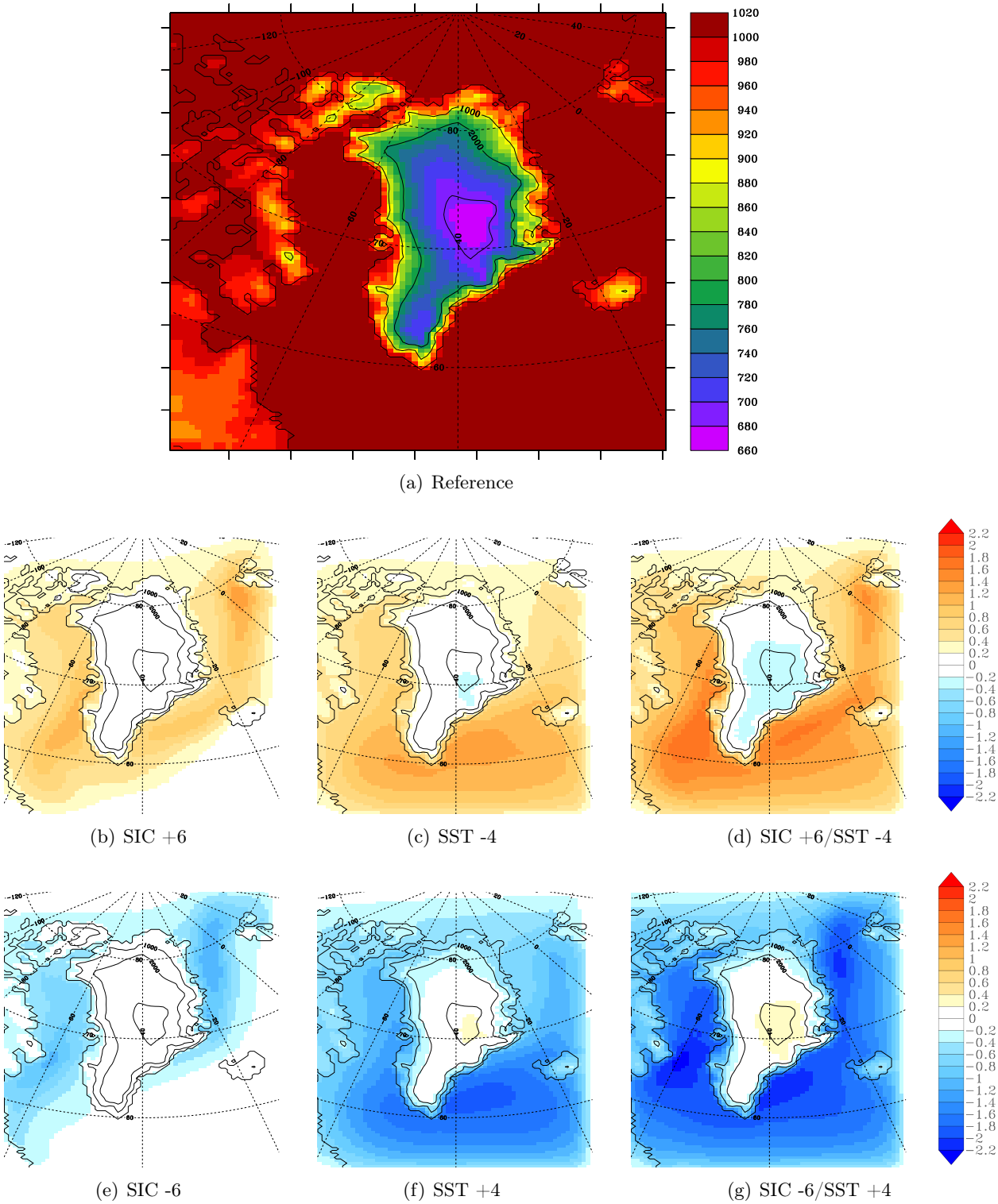

(a) Reference

(b) SIC +6

(c) SST -4

(d) SIC +6/SST -4

(e) SIC -6

(f) SST +4

(g) SIC -6/SST +4

Fig. 9. Annual mean surface pressure (hPa) for the reference run (a) over 2007–2012. Difference in annual mean surface pressure (hPa) between (b) SIC +6, (c) SST -4, (d) SIC +6 / SST -4, (e) SIC -6, (f) SST +4, (g) SIC -6/SST +4 experiments and the reference run.

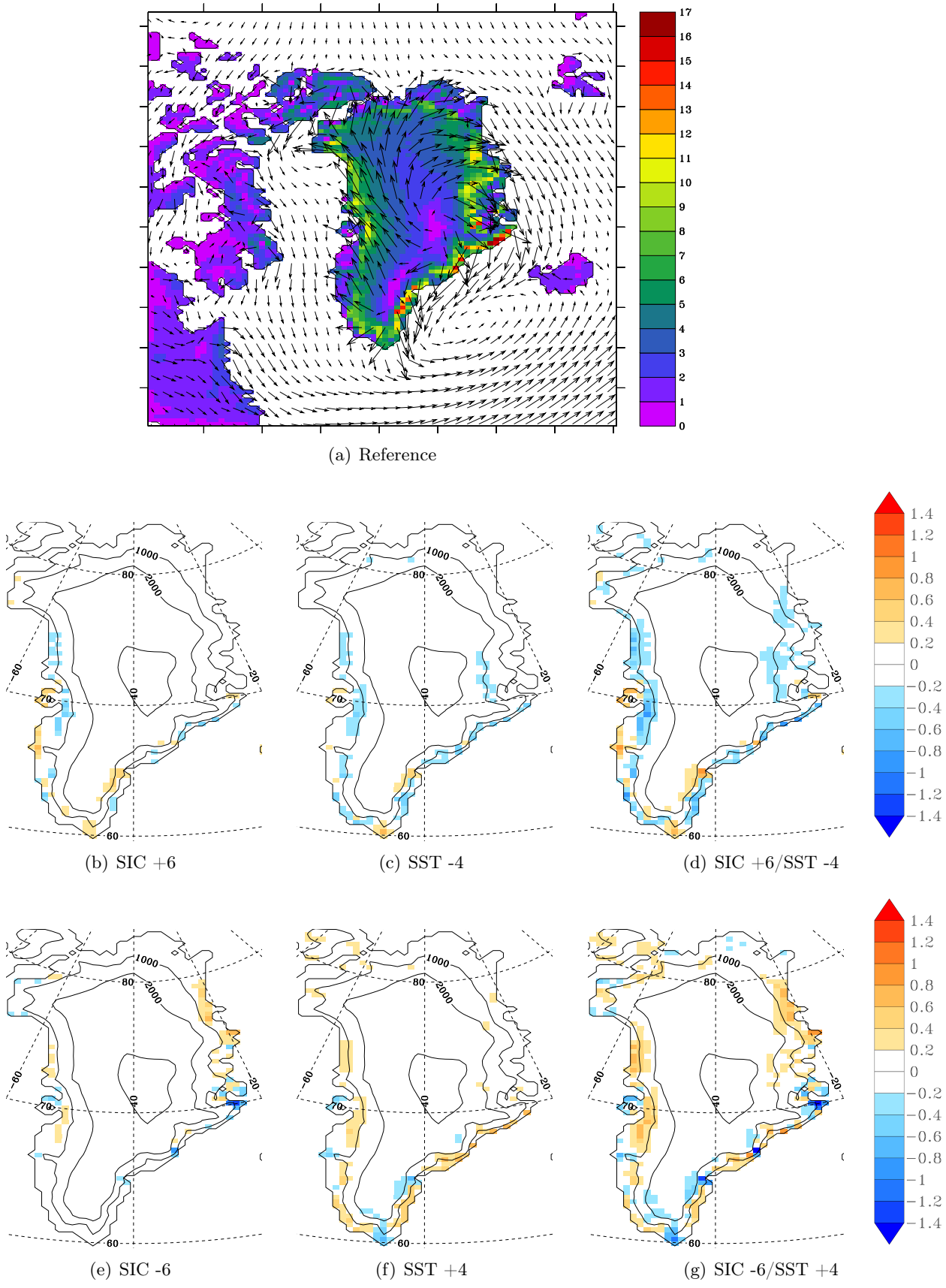

(a) Reference

(b) SIC +6

(c) SST -4

(d) SIC +6/SST -4

(e) SIC -6

(f) SST +4

(g) SIC -6/SST +4

Fig. 10. Annual mean wind speed (m/s) for the reference run (a) over 2007–2012. Difference in the annual mean wind speed (m/s) between (b) SIC +6, (c) SST -4, (d) SIC +6/SST -4, (e) SIC -6, (f) SST +4, (g) SIC -6 / SST +4 experiments and the reference run.